Environmental Science and Pollution Research (2019) 26:22656–22669
https://doi.org/10.1007/s11356-019-05556-6

RESEARCH ARTICLE

Highly porous carboxylated activated carbon from jute stick for removal of Pb^{2+} from aqueous solution

Md. Abdul Aziz[1] · Imran Rahman Chowdhury[2] · Mohammad Abu Jafar Mazumder[3] · Shakhawat Chowdhury[2]

Received: 3 January 2019 / Accepted: 23 May 2019 / Published online: 5 June 2019

Abstract

Drinking water is a potential source of human exposure to lead (Pb^{2+}), which can induce several health effects upon exposure to low dose for a long period. In particular, the children and young populations are the vulnerable groups. Removal of Pb^{2+} from drinking water using an inexpensive adsorbent is a challenge. In this research, activated carbon adsorbent was developed using jute stick, an agricultural by-product. Following carboxylic acid functionalization, the jute stick activated carbon (JSAC) was applied for Pb^{2+} removal from aqueous solution. The carboxylated JSAC (JSAC-COO^-) was characterized using several techniques. The surface area of the JSAC-COO^- was 615.3 m^2/g. The JSAC-COO^- was tested for variable concentrations of Pb^{2+} (10 and 25 mg/L) at different pH (4.0 and 7.0), temperature (15 °C and 27 °C), and contact periods (1, 5, 10, 15, 30, and 60 min). Up to 99.8% removal of Pb^{2+} was achieved for these concentrations of Pb^{2+} within 15 min of contact time. The adsorption process followed standard kinetics, and the adsorption capacity was > 25.0 mg Pb^{2+}/g of JSAC-COO^-. The JSAC-COO^- can be used for fast and easy removal of Pb^{2+} from aqueous solution, which has the potential for domestic and industrial applications.

Keywords Lead removal · Carboxylated jute stick activated carbon · Adsorbent · Drinking water · Domestic and industrial applications

Introduction

The metals with density of 5 g/cm^3 or higher are characterized as heavy metals. Heavy metals in water is one of the major environmental issues as they are toxic to human and ecological health. Lead (Pb) has an atomic weight and density of 207.2 g and 11.4 g/cm^3, respectively (José and José 2006). It forms a wide range of oxides (e.g., Pb_2O to PbO_2) and a protective film on the exposed surface (José and José 2006). It is one of the toxic heavy metals that pose risk to humans and aquatic lives, even at a low concentration for a long period of exposure (Martins et al. 2006). The children and young populations are the most vulnerable groups for exposure to Pb in water. The International Agency for Research on Cancer (IARC) has classified Pb as group 2B (possible human carcinogen) and inorganic compounds of Pb as group 2A (probable human carcinogen) while the USEPA has classified Pb as group B2 (probable human carcinogen) (IARC 2018; USEPA 2004). The World Health Organization (WHO) and European Community Directive have set the guideline value to 10 μg/L in drinking water (WHO 2011). The Health Canada has set the maximum acceptable concentration to 10 μg/L in drinking water (Health Canada 2015). The USEPA has the action level of 15 μg/L in drinking water (USEPA 2009).

Lead is a naturally occurring element, mainly buried in the Earth's crust in insoluble and biologically inoffensive forms. It is generally found as PbS or as complex ores of Pb and zinc sulfides with small fractions of silver or silver sulfides (USEPA 2012; WHO 2003). Due to industrialization and biogenic activities, large quantities of Pb and by-products are released into air, soil, and water. It is primarily used as raw

Responsible editor: Tito Roberto Cadaval Jr

✉ Shakhawat Chowdhury
SChowdhury@kfupm.edu.sa

[1] Center of Research Excellence in Nanotechnology (CENT), King Fahd University of Petroleum and Minerals, Dhahran 31261, Saudi Arabia

[2] Department of Civil and Environmental Engineering, King Fahd University of Petroleum and Minerals, Dhahran 31261, Saudi Arabia

[3] Chemistry Department, King Fahd University of Petroleum and Minerals, Dhahran 31261, Saudi Arabia

materials in the manufacturing industries (e.g., matches, explosives, pigments, storage batteries, paints, and fuels) that produce lead-contaminated wastewater and air (e.g., smelting/grinding industries), which are the major sources of water pollution for drinking water supplies. As an example, Pb concentrations in wastewater from the battery manufacturing, acid mine drainage, tailing pond, and steel production plants were reported to be in the range of 0.5–25 mg/L (Patterson 1985).

Chronic exposure to Pb in drinking water can induce multiple health effects (Davis 1990). Lead has the bioaccumulation and magnification properties, which can increase its concentrations to toxic levels (Atkinson et al. 1998). It can affect almost every organ and system in the body while the children below 6 years are the most vulnerable group to the effects of Pb (Wani et al. 2015). Low concentrations of Pb in blood can cause several problems including, hearing, learning and behavior problems, slow growth, lower intelligence quotient, and hyperactivity (Banerjee et al. 2007; Bellinger 2008; Fraser et al. 2006). It can cross the placental barrier during pregnancy, which may result in serious effects (e.g., reduced growth of the fetus; premature birth) to the mother and the developing fetus (Bellinger et al. 1987). The adults exposed to Pb can suffer from cardiovascular effects, increased blood pressure and hypertension, decreased kidney function, and reproductive problems (Benjelloun et al. 2007; Navas-Acien et al. 2007; Patrick 2006; Wani et al. 2015). Consumption of elevated levels of Pb increases the reactive oxygen species (ROS) in tissues, which can affect the reproduction system in male and metabolism process and damage the cellular components (Patrick 2006).

Removal of Pb ions (Pb^{2+}) from drinking water at low cost has been an issue. To remove Pb^{2+} from aqueous solution, various methods including coagulation, adsorption, membrane filtration, ion exchange, chemical precipitation, and reverse osmosis have been employed (Meunier et al. 2006; Mohamed et al. 2008; Merzouk et al. 2008; Yu et al. 2006). Among the methods, adsorption has been the method of choice, due mainly to the low cost, high efficiency, and easy to use (Chowdhury et al. 2016). The activated carbon-based adsorbents have been widely used for Pb^{2+} removal (Chowdhury et al. 2016). Many studies have developed and applied activated carbon from different sources, including rice husk (Khalid et al. 1998), rice straw (Johns et al. 2003), discarded automotive tires (Netzer and Hughes 1984), rubber wood sawdust (Kalavathy et al. 2005), apricot stone (Kobya et al. 2005), peanut shell (Wilson et al. 2006), pecan shell (Guo and Rockstraw 2007), crab shell (Lee et al. 1998), fly ash (Gupta et al. 1998; Weng and Huang 1994), peat (Gosset et al. 1986; Chaney and Hundemann 1979), and oil palm fiber (Tan et al. 2008) to remove Pb^{2+} from aqueous solution.

The non-toxic agriculture by-products are generally the preferred options for preparing adsorbents. However, finding the inexpensive and non-toxic raw materials for developing the activated carbon is a challenge. There is need to select a non-toxic, inexpensive, and available raw materials to produce activated carbon for Pb^{2+} removal from drinking water. Jute stick, a residue of jute, is an agricultural by-product, which is cheap and abundant in Bangladesh, India, Thailand, Myanmar, and China. The jute fiber has been reported to be biodegradable and environmentally friendly (FAO 2019). The jute stick and jute fiber have similar chemical constituents indicating that the jute stick is likely to be biodegradable and environmentally friendly (Mitra 1999), which is commonly used as the raw materials for cooking in the rural areas.

The biomass-based activated carbon needs to have large specific surface area, functional groups and increased accessibility of heavy metals to the intra-pore space. As an example, Anitha et al. (2015) reported that the carboxylate-functionalized carbon nanotube ($CNT–COO^-$) surface effectively adsorbed 150–230% more metal ions than the non-functionalized CNT surface. This study reported higher efficiency of $CNT–COO^-$ than the hydroxyl and amide-functionalized CNTs for Cd^{2+} removal, due possibly to the high negative charge of $CNT–COO^-$, leading to higher affinity to heavy metals while the performance was sensitive to pH. However, carboxylation of CNTs and activated carbon (e.g., date palm derived carbon) reduced the specific surface area significantly (El-Shafey et al. 2016), indicating the needs of carboxylate-functionalized carbon materials with high surface area for heavy metal removal. The biomass is treated with different activation agents, such as H_3PO_4, NaOH, $ZnCl_2$, K_2CO_3, $KHCO_3$, and KOH to obtain variable surface area, pore size, and shape of the carbon materials prior to pyrolysis (Ahammad et al. 2019). Although activated carbon prepared from jute stick was investigated to remove heavy metals from industrial wastewater (Asadullah et al. 2014), the effect of carboxylate-functionalized jute stick activated carbon on removal of heavy metals has not been investigated yet. It is anticipated that the carboxylate-functionalized jute stick activated carbon be investigated for heavy metal removal from aqueous solution. In this study, a highly porous carbon material (jute stick activated carbon (JSAC)) was developed from jute stick using $NaHCO_3$ as the activation agent. The JSAC was used for Pb^{2+} removal from aqueous solution. The carboxylation was performed using acid treatment. Material characterization was performed using field-emission scanning electron microscopy (FESEM), energy-dispersive spectroscopy (EDS), Raman spectroscopy, X-ray diffraction (XRD) spectroscopy, Fourier transform infrared spectroscopy (FT-IR), and BET surface area analyzer. The carboxylate-functionalized JSAC (JSAC-COO^-) was tested through batch experiments with variable concentrations of Pb^{2+} (10 and 25 mg/L) at different pH (4.0 and 7.0), temperature (15 °C and 27 °C) and contact periods (1, 5, 10, 15, 30, and 60 min). The adsorption kinetics was investigated. The performance of

JSAC and JSAC-COO^- was discussed, and the feasibility of using JSAC-COO^- in removing Pb^{2+} from aqueous solution was highlighted. The needs for carboxylation of JSAC was demonstrated through conducting the Pb^{2+} removal experiments. The Pb^{2+} removal performance of JSAC was significantly lower than that of the JSAC-COO^-.

Methodology

Raw materials

The jute sticks were collected from Mominpur, Jessore (Bangladesh). The main constituents of jute fibers are 58–63% α-cellulose, 20–22% hemicellulose, and 12–14% lignin (Islam et al. 2003). Table 1 shows the physical and chemical characteristics of jute stick. The non-cellulosic constituents are 37–42% while the chemical composition is similar to jute fiber. The jute stick contains higher lignin (23.5%) and lower α-cellulose (40.8%) than jute fiber (Islam et al. 2003). The reagents (e.g., $NaHCO_3$, hydrochloric acid (HCl, 37 *w*/*v*%), sulfuric acid (H_2SO_4), nitric acid (HNO_3), Pb standard solution (1000 ppm (ppm), and other chemicals) were obtained from Sigma-Aldrich. The deionized water was obtained from the water purification system (Barnstead Nanopure, Thermo Scientific, 7148, USA).

Preparation of JSAC

The jute sticks were cut into small pieces with chopper and cleaned with deionized water (DIW). The cleaned sticks were dried at 110 °C in an oven for 24 h. The dried sticks were powdered by a household blender. The powder was mixed with $NaHCO_3$ with a mass ratio of 1:4 by a household blender. The mixture was placed in the middle of tube furnace and heated at 850 °C for 5 h under nitrogen atmosphere (Fig. 1). The heating and cooling rates were 5 °C/min and 10 °C/min, respectively. The carbon was washed twice with DIW and 0.5 M HCl, and dried. Finally, the product (JSAC) was dried at 60 °C in a vacuum oven to constant weight. The schematic procedure for the preparation of activated carbon (JSAC) is described in Fig. 1.

Table 1 Properties of jute stick

	Type	Quantity
Bulk density (kg/m^3)		178.84
Gross calorific value (MJ/kg)		17.32
Proximate analysis (%)	Volatile	78.40
	Fixed carbon	11.80
	Moisture	9.02
	Ash	0.78
Ultimate analysis (%)	C	44.94
	H	4.38
	N	
	O	49.90

Carboxylation of JSAC

The reaction scheme for carboxylation of the JSAC is described in Fig. 2. Briefly, a total of 2.4 g porous JSAC was added to 1.6 L mixed solution of concentrated H_2SO_4 and HNO_3 (3:1 by volume), and the solution was transferred to ultrasonicator. Following sonication for 5 h to generate carboxylic groups, the reaction mass was diluted with DIW. The resultant diluted mixture was kept standstill for 8 h to form separate layers between carboxylated carbon and mother liquor. Then, the upper layer (mother liquor) was decanted. The dilution and decantation procedure was repeated six times. After filtering and washing with DIW, the carboxylate-functionalized JSAC (JSAC-COO^-) were dried at 60 °C for 24 h.

Instrumentation

The field-emission scanning electron microscopy (FESEM) image of the carboxylated JSAC (JSAC-COO^-) was taken by an FESEM, TESCAN LYRA 3, Czech Republic. An Oxford Instruments Xmass detector equipped with the FESEM was used for the determination of energy dispersive X-ray spectra (EDS). An iHR320 with CCD detector, HORIBA, Raman spectrometer equipped with green laser (300 mW) excitation wavelength λ_o = 532 nm, was used for the study and detection of graphite structure in the JSAC-COO^-. The X-ray diffraction analysis and chemical analysis of JSAC-COO^- were obtained by a high-resolution Rigaku Ultima IV X-ray diffractometer equipped with Cu-K (alpha) radiation and an XPS equipped with an Al K-alpha micro-focusing X-ray monochromator (ESCALAB 250Xi XPS Microprobe, Thermo Scientific, USA), respectively. A Perkin Elmer (16F PC FTIR) spectrometer was used for recording FTIR spectra. The Micromeritics ChemiSorb 2750 was used for the BET and Barrett–Joyner–Halenda (BJH) analyses to measure the surface area and pore size of the JSAC-COO^-. A Power sonic 603 ultrasonic cleaner was used for sonication. The pH of the buffer solutions was recorded using a dual channel pH meter (XL60, Fisher Scientific).

Sample preparation and analysis

Figure 3 shows the summary of batch experiments. The Pb^{2+} standard solution, 1000 ppm Pb^{2+} in 0.5 M HNO_3

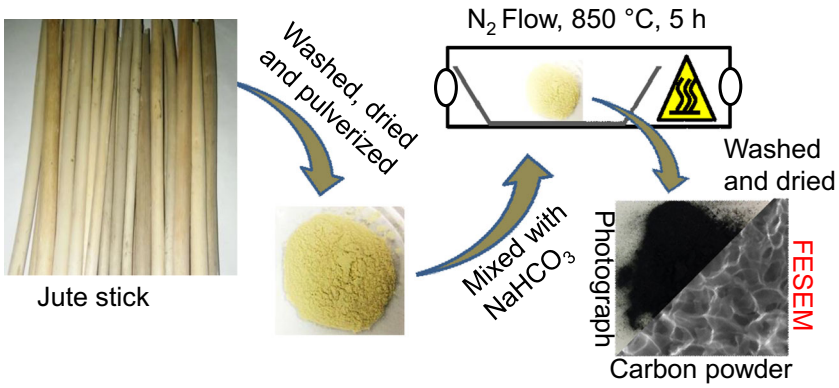

Fig. 1 Preparation of porous activated carbon from jute stick

from $Pb(NO_3)_2$, was purchased from Sigma-Aldrich and used as a stock solution to prepare the diluted solutions of the required concentrations (10 and 25 mg/L). The pH of the solution was adjusted to 4.0 and 7.0 using 0.1 M NaOH and 0.1 M HNO_3. The temperature was controlled using the temperature-controlled oil bath. Twenty milligrams of the JSAC-COO^- was added into 20 mL solution with Pb^{2+} concentrations in the range of 10–25 mg/L in a screw cap glass vial. The upper limit of Pb^{2+} concentration of 25 mg/L was selected following Patterson (1985). However, the range of concentrations can be increased depending on the Pb^{2+} concentrations in the aqueous solution. The solutions were stirred at 200 rpm, and the sorption reactions were allowed for 1, 5, 10, 15, 30, and 60 min prior to filtration using 0.45 μm filter paper.

The filtered Pb^{2+} samples were analyzed using the inductively coupled plasma-mass spectrometer (ICP-MS) (Model: ICP-MS XSERIES-II) following USEPA Method 6020A (USEPA 1998). The ICP-MS was calibrated using the blank and four different concentrations of Pb(II). The analysis was replicated three times, and averages were taken as the residual concentrations of Pb^{2+}. The detection limit of ICP-MS is 0.05 parts per billion (USEPA 1998).

Results and discussion

Structure and morphology

Figure 4a and b show the FESEM images of the JSAC-COO^-. Figure 4b shows the size of carbon particles in the range of few μm to 60 μm. However, the magnified view shows that each microparticle is composed of numerous nanosheets (Fig. 4a). All nanosheets exist in regular arrangement with an extensive quantity of uniform size macropores in the JSAC-COO^-. For clear presentation, some nanosheets (in the rectangular boxes) and macropores (in the circles) are shown in Fig. 4a. The uniform and large number of macropores increased the surface area significantly. The unique architecture of nanosheets with large interlayer spacing is suitable for heavy metal removal. The EDS spectrum (Fig. 4c) of JSAC-COO^- shows the presence of C, O, and Sn, which are expected as the JSAC-COO^- was immobilized on fluorine-doped tin oxide prior to recording the EDS spectrum. It indicates that the JSAC-COO^- is composed of carbon and oxygen. For comparing morphology and chemical composition, the SEM images and EDS spectrum of JSAC were also recorded (Fig. 4d, e). The morphology and chemical composition of JSAC-COO^- and JSAC were similar. However, the ratio of oxygen to

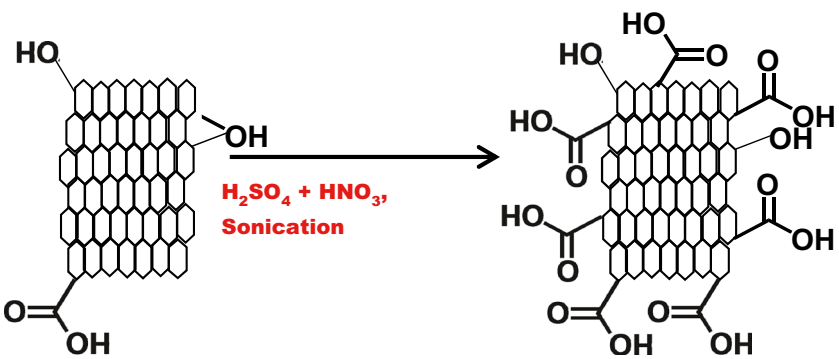

Fig. 2 Carboxylation of the porous activated carbon

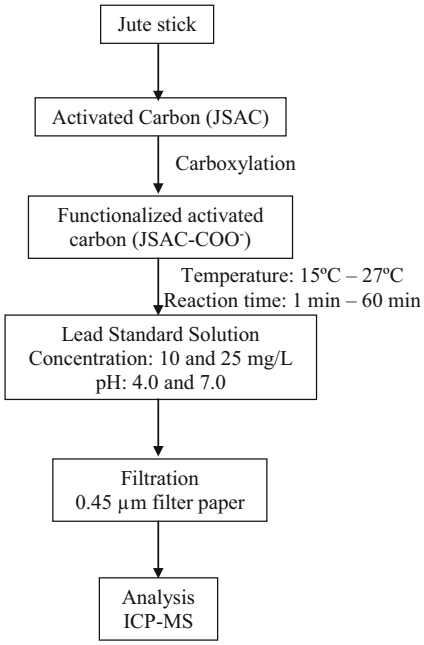

Fig. 3 Summary of batch experiment

carbon peak intensity of JSAC-COO$^-$ (Fig. 4c) was much higher than that of JSAC (Fig. 4d). This indicates that additional oxygen molecules were introduced into the JSAC during carboxylation.

Figure 5a shows the XRD spectrum of JSAC-COO$^-$ at 850 °C. All the diffraction peaks can be assigned to the porous graphitic framework (JCPDS no. 41-1487) with two broad peaks at around 2θ = 25° and 43°, corresponding to carbon (002) and (101) peaks, respectively (Quan et al. 2012). The XRD pattern indicates that graphite structure was obtained after carboxylation of JSAC. However, broadening of the two peaks indicates the low degree of graphitization, i.e., small domains of coherent and parallel stacking of graphene. Figure 5b shows the Raman spectrum of JSAC-COO$^-$. The spectrum consists of two broad peaks; centered at around 1589 and 1335 cm^{-1}, which are caused by the effects of graphitization (G) and defects (D), respectively (Li et al. 2017). Moreover, the intensity of D-band is higher than the intensity of G-band, indicating that there are some defects and interspaces on the surface of carbon (Li et al. 2017).

Functional groups

The functional groups of JSAC-COO$^-$ were evaluated using the XPS and FTIR measurements. Figure 6a shows the XPS survey scan spectrum, indicating three major bands at approximately 284.60, 486.60, and 531.60 eV representing C1s, Sn3d, and O1s, respectively. The peak for Sn is due to the use of fluorine-doped tin oxide (FTO) substrate for developing JSAC-COO$^-$ sample for XPS analysis. This finding is consistent with the EDS in Fig. 4c. The C1s core level spectrums consist of two major peaks at around 284.60 and 288.60 eV (Fig. 6b), which are associated with carbon in the states of C–C and $^-$O–C=O, respectively (Wang et al. 2014). The position and pattern of the peaks are consistent to C1s peaks of carboxylated carbon materials (Aziz and Yang 2008; Adenuga et al. 2013). To compare the functional group, the XPS spectra of JSAC was recorded. The survey spectrum of JSAC (spectrum not shown) showed that JSAC was composed of carbon and oxygen like JSAC-COO$^-$. However, the typical peak of $^-$O–C=O functional group at around 288.60 eV in the C1s core level spectrums (Fig. 4c) of JSAC was absent while the peak at around 284.60 eV for C–C of the JSAC was present. The types of oxygenated functional group in the JSAC are described with the FTIR data below.

Figure 6d shows the FTIR spectrum of JSAC-COO$^-$. The characteristic absorption bands at 3866.2, 3440.3, 2922.8, 2852.0, 2354.8, 1723.5, 1618.0, 1458.0, 1390.2, 1251.0, 1124.3, 1026.8, 668.5, 522.4, and 431.1 cm^{-1} indicated the carbon materials containing several functional groups. The broad peak at 3440.3 cm^{-1} indicated the presence of –OH group, which is primarily a characteristic peak of carboxylic functionality (Tejada et al. 2016; Adenuga et al. 2013). Absorption peak at 1724 cm^{-1} was assigned to C=O stretch of COOH in JSAC-COO$^-$; the symmetric and antisymmetric stretching of COO$^-$ appeared at 1618 and 1458 cm^{-1}, respectively (Tejada et al. 2016; Adenuga et al. 2013). In addition, the peaks appeared at 1458.0 and 1026.8 cm^{-1} could be assigned to vibration of carboxylic acids (Tejada et al. 2016). Besides, the peaks at 2922.8 and 2852.0 cm^{-1} suggested the presence of C–H functional groups in JSAC-COO$^-$.

Figure 6e shows the FTIR spectrum of JSAC. The characteristic absorption bands at 3750, 3440, 2922, 2852, 2358, 1618, 1564, 1396, 1101, 636, and 465 cm^{-1} indicated the carbon materials containing several functional groups. The broad absorption at 3433.3 cm^{-1} indicated the presence of –OH group. The peaks at 2922, 2852 cm^{-1} suggested the presence of C–H functional groups. Absorption peaks at 1618 and 1564 cm^{-1} were assigned to C=C stretch. In addition, the peaks appeared at 1101 cm^{-1} may indicate the presence of C–O functional group. However, the absorption peak at 1724 cm^{-1} was absent in JSAC (Fig. 6e), unlike Fig. 6d, which is related to C=O stretch of COOH. This clearly indicates that the JSAC was successfully functionalized with carboxylic groups as JSAC-COO$^-$. The above findings corroborated with XPS results (vide supra) (Fig. 6a–c).

Surface area evaluation

Figure 7a shows the nitrogen adsorption–desorption isotherms for JSAC-COO$^-$. The Brunauer–Emmett–Teller (BET) analysis indicated a type II adsorption–desorption isotherm with a high nitrogen adsorption–desorption capacity. The sample

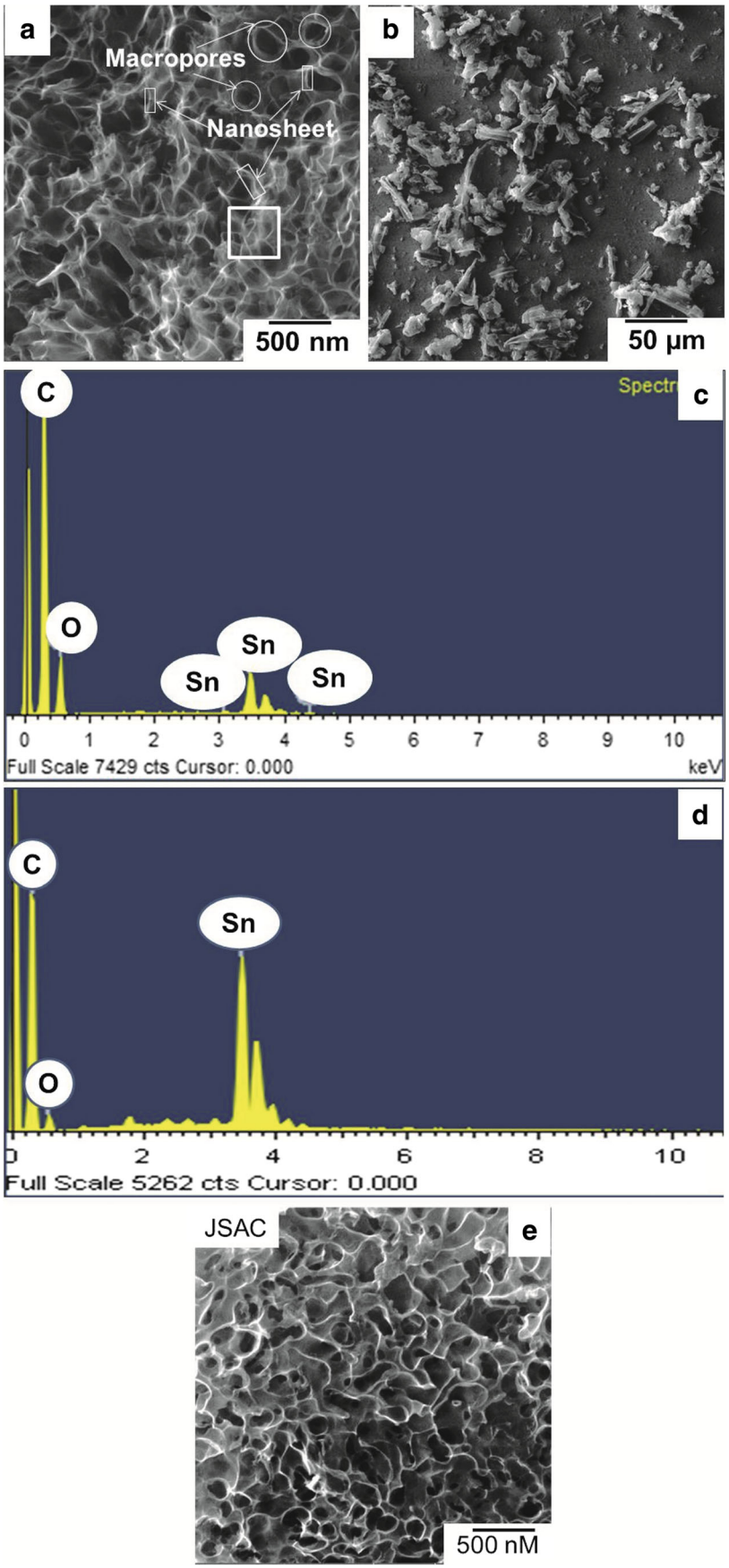

Fig. 4 **a**, **b** FESEM images of the JSAC-COO^{-}. **c** EDS spectrum of the white marked area of **a**. **d** EDS spectrum of the JSAC. **e** FESEM images of JSAC

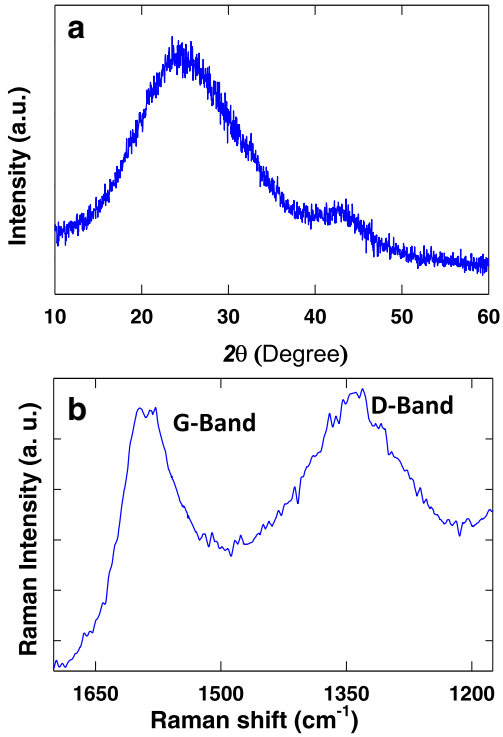

Fig. 5 **a** X-ray diffraction and **b** Raman spectrum of the JSAC-COO$^-$

shows a broader hysteresis loop from $P/P_0 = 0.4$ to $P/P_0 = 1$ indicating the presence of mesopores (Thommes et al. 2015). Besides, a decent increase of hysteresis loop in the high relative pressure range (P/P0 = 0.80–1.00) indicates the presence of macropores (Thommes et al. 2015; Sun et al. 2018). The BET surface area and total pore volume of JSAC-COO$^-$ nanosheets were found to be 615.3 m^2/g and 0.3677 cm^3/g, respectively. The BET surface area of JSAC-COO$^-$ was found to be lower than that that of JSAC prior to functionalization (1142.4 m^2/g). Oxidation of carbon materials with acid has increased the surface hydrophilicity via the insertion of carbon oxygen polar that occupied large fraction of the surface (El-Shafey et al. 2016). The large amounts of these groups have reduced the adsorption of non-polar nitrogen molecules, which has lowered the BET surface area (El-Shafey et al. 2016). Table 2 presents the BET surface area before and after functionalization of few carbon materials. The surface area of JSAC-COO$^-$ is significantly higher than other carboxylated carbon materials including activated carbon prepared from date leaves, carbon nanotube, and graphene (Table 2).

Figure 7b shows the BJH pore-size distribution of JSAC-COO$^-$. This represents a wide distribution of pore width (range 1.7 to 150 nm) with a BJH adsorption average pore width of 8.93 nm. The range of pore size, average pore width, and type of the curve (Fig. 7b) indicate large fractions of mesopores and micropores in JSAC-COO$^-$ (Thommes et al. 2015). Overall, the BET analysis confirmed the presence of macro- and mesopores in addition to micropores in JSAC-

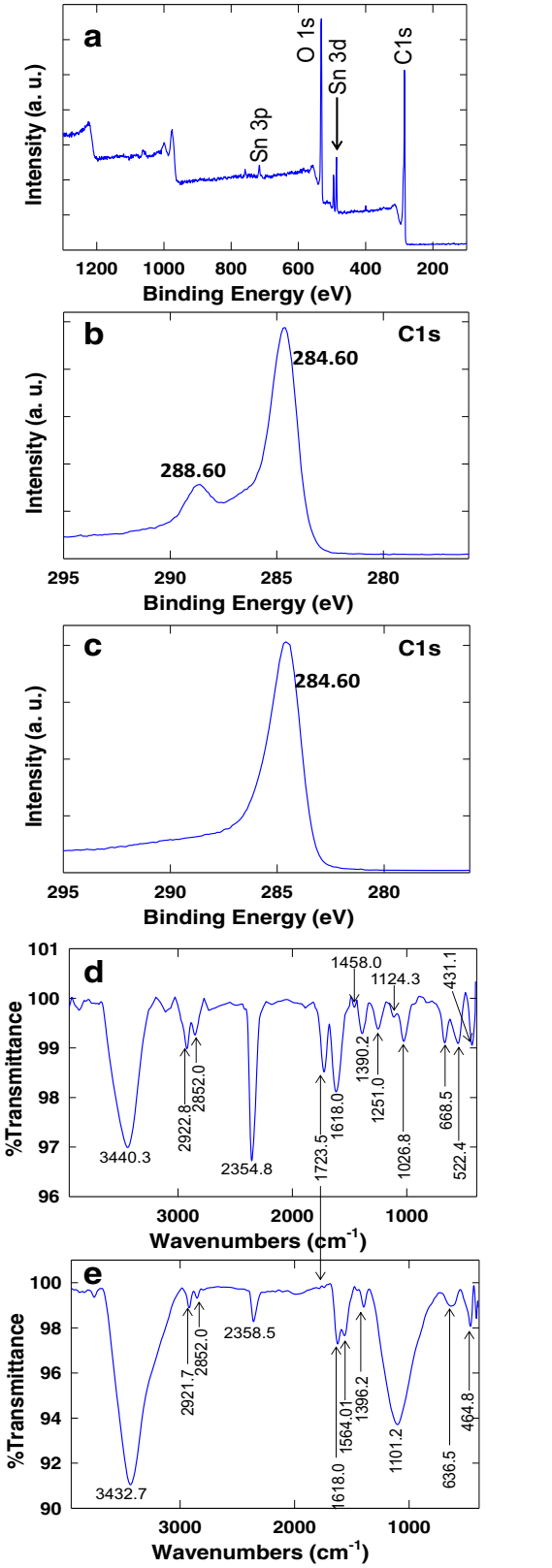

Fig. 6 **a** XPS survey spectrum of the JSAC-COO$^-$ with three major peaks of carbon, oxygen, and tin. High-resolution spectrum of C1s zone of **b** JSAC-COO$^-$ and **c** JSAC. FTIR spectrum of the **d** JSAC-COO$^-$ and **e** JSAC

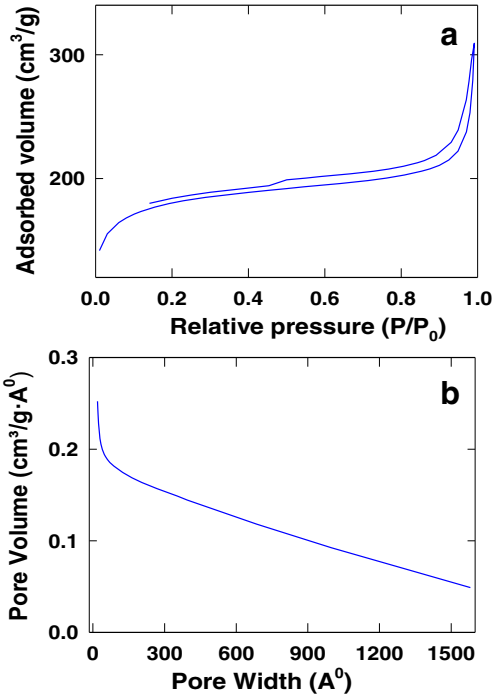

Fig. 7 **a** Nitrogen adsorption–desorption isotherm and **b** corresponding BJH pore-size distributions of JSAC-COO^-

COO^-, which is reflected in microscopic analysis (Fig. 4). The combination of macro- and mesoporous structure increased the specific surface area and offered increased sites for ion mobility (Sun et al. 2018). In general, coexistence of macro- and mesopores leads to highly porous structure and large specific surface area while the carboxylic functional group plays a vital role for removal of heavy metals from drinking water. Consequently, the JSAC-COO^- is considered as a potential candidate for Pb^{2+} removal from drinking water.

Removal of Pb^{2+}

Adsorption kinetics

The concentrations of Pb^{2+} following adsorption onto JSAC-COO^- at different contact periods are shown in Fig. 8. Within 1.0 min of contact period, Pb^{2+} removal was obtained to be in the range of 90.8–97.7% for different initial concentrations at varying temperature and pH (Fig. 8a, b). For the initial concentration of 10 mg/L, concentrations of Pb^{2+} were reduced to 0.67 and 0.23 mg/L for pH of 4.1 and 6.9, respectively (Fig. 8a). At initial concentration of 25 mg/L, concentrations of Pb^{2+} were reduced to 2.13 and 0.93 mg/L for pH 4.2 and 6.9, respectively. In these experiments, temperature was maintained at 27 °C. At 15 °C, the corresponding removal rates were found to be lower (Fig. 8c, d).

Following the rapid drop of Pb^{2+} concentration in water after the 1st minute, the remaining Pb^{2+} concentrations showed gradual decrease. At higher pH and temperature, final concentrations of Pb^{2+} were much lower than for the lower pH and temperature. At pH and temperature of 4.2 and 15 °C, respectively, Pb^{2+} concentrations were reduced from 25 mg/L to less than 10 μg/L in 60 min. At pH and temperature of 6.9 and 15 °C, Pb^{2+} were reduced to below 10 μg/L in 30 min. When pH and temperature were 6.9 and 27 °C, respectively, Pb^{2+} were decreased to less than 10 μg/L in 15 min. The final concentrations of Pb^{2+} showed exponential delay in all scenarios. At pH and temperature of 4.1 and 27 °C, respectively, final concentrations of Pb^{2+} from the initial of 10 mg/L were represented by the exponential relationship as:

$$C = 2.4932e^{-0.244t} \quad (1)$$

Table 2 Comparison of BET surface area of before and after carboxylate functionalization of different carbon materials

No.	Name of the carbon materials	Oxidizing agent	BET surface area of before carboxylate functionalization (m^2/g)	BET surface area of after carboxylate functionalization	Reference
1	Single-walled CNTs	Refluxed in 5 M HCl	55.2641	6.5824	Lekgoathi et al. (2008)
2	Vulcan XC72R	Concentrated HNO_3	241	167	Carmo et al. (2009)
3	Multi-walled CNT (MWCNT)	Mixture of concentrated H_2SO_4 and HNO_3	298	266	Cañete-Rosales et al. (2012)
4	Date palm leaflets derived AC	Concentrated HNO_3	823	33.8	El-Shafey et al. (2016)
5	Multi-walled CNT	Concentrated HNO_3	170	130	Burmistrov et al. (2016)
6	Multi-walled CNT	Mixture of HNO_3 and H_2O_2	–	194.4	Farghali et al. (2017)
7	Jute stick derived activated carbon	Mixture of concentrated H_2SO_4 and HNO_3	1142.4	615.3	This work

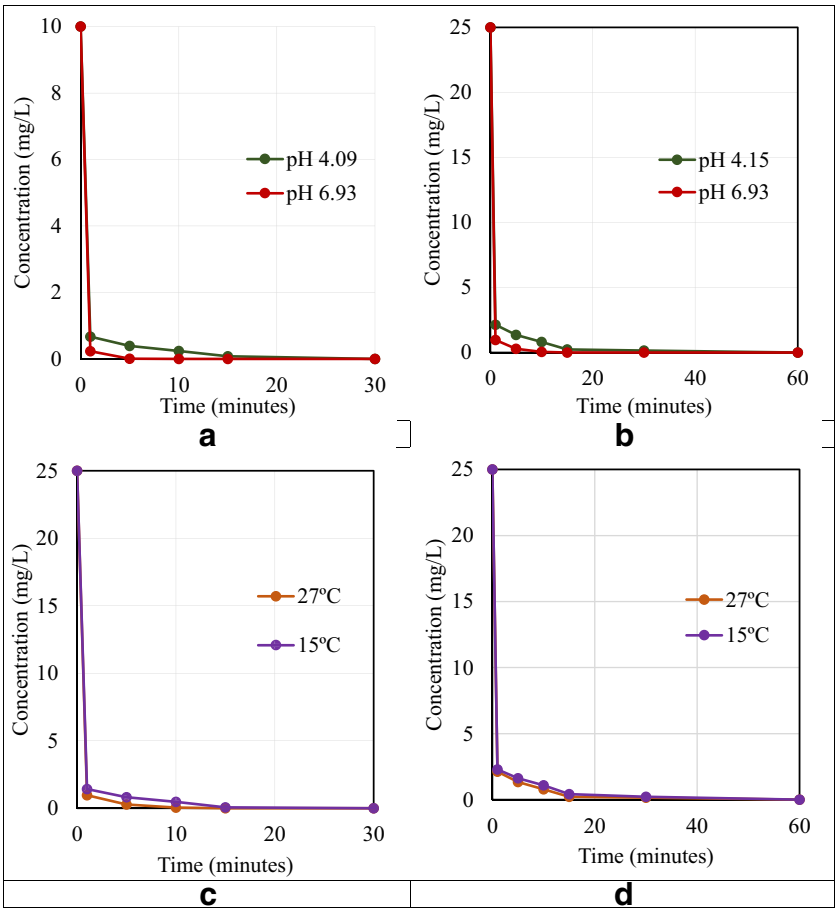

Fig. 8 Effect of contact time on adsorption of Pb^{2+} by JSAC-COO^{-}. **a** Initial concentration 10 mg/L, temperature 27 °C. **b** Initial concentration 25 mg/L, temperature 27 °C. **c** Initial concentration 25 mg/L, pH 6.93. **d** Initial concentration 25 mg/L, pH 4.15

where C = concentration of Pb^{2+} (mg/L) and t = time (min). The relationship had $R^2 = 0.73$, and it was valid for up to 15 min. Beyond this period, concentrations of Pb^{2+} were below the detection limit.

At pH of 6.9, final concentrations of Pb^{2+} from the initial concentration of 10 mg/L were represented by the exponential relationship as:

$$C = 3.3451e^{-1.307t} \quad (2)$$

The relationship had R^2 of 0.88, and it was valid for up to 5 min. Beyond this period, concentration of Pb^{2+} were below the detection limit.

For pH and temperature of 4.2 and 27 °C, respectively, final concentrations of Pb^{2+} from the initial concentration of 25 mg/L were represented by the exponential relationship as:

$$C = 4.4641e^{-0.136t} \quad (3)$$

The relationship had R^2 of 0.70, and it was valid for up to 30 min. Beyond this period, concentration of Pb^{2+} were below the detection limit.

At pH of 6.9 and temperature of 27 °C, the exponential decay relationship was

$$C = 5.9828e^{-0.516t} \quad (4)$$

The relationship had R^2 of 0.80, and it was valid for up to 10 min. Beyond this period, concentration of Pb^{2+} were below the detection limit.

For pH and temperature of 4.2 and 15 °C, respectively, final concentrations of Pb^{2+} from the initial concentration of 25 mg/L were represented by the exponential relationship as:

$$C = 5.0313e^{-0.121t} \quad (5)$$

The relationship had R^2 of 0.70, and it was valid for up to 30 min.

For pH and temperature of 6.9 and 15 °C, respectively, final concentrations of Pb^{2+} from the initial concentration of 25 mg/L were represented by the exponential relationship as:

$$C = 6.3706e^{-0.297t} \quad (6)$$

The relationship had the R^2 of 0.79, and it was valid for up to 15 min. In all scenarios, the final concentrations of Pb^{2+} showed exponential decay while the effects of pH and temperature were found to be dominant beyond the 1st minute of contact period.

Pb^{2+} removal and interaction effects

The adsorbent JSAC-COO^- showed more than 98.3% removal of Pb^{2+} in 15 min of contact period for variable initial concentrations, temperature, and pH (Fig. 8). The interaction effects of pH and temperature are shown in Fig. 9. At higher pH and temperature, Pb^{2+} removal efficiency was higher. The parallel lines of efficiencies for different temperature for up to 10 min showed minimum/no interaction effect between pH and temperature while both were showing increasing trends for removal of Pb^{2+} ions at higher pH (Fig. 9). However, after 10 min, increase in temperature and pH showed the decrease in the rates of removal, which might be due to the very low concentrations of Pb^{2+} ions in the aqueous solution after 10 min. It is to be noted that more than 98.0% removal of Pb^{2+} ions was achieved by this time.

At 15 °C, increase of pH from 4.2 to 6.9 increased the removal efficiency from 90.8 to 94.3% in the 1st minute. For the contact periods of 5, 10, and 15 min, the removal efficiencies increased from 93.5 to 96.7%, 95.6 to 98.1%, and 98.3 to 99.7%, respectively. At 27 °C, increase of pH from 4.2 to 6.9 increased the removal efficiency from 91.5 to 96.2% in the 1st minute. The removal efficiencies were increased from 94.6 to 98.9% and 96.8 to 99.8% in 5 and 10 min of contact periods, respectively (Fig. 9). In this study, the JSAC-COO^- adsorbents reduced Pb^{2+} ions from an initial concentration of 25 mg/L to meager concentrations of 10 μg/L within 15–60 min of contact period depending on pH and temperature while more than 90% removal of Pb^{2+} was achieved within the 1st minute of contact period. Overall, the removal of Pb^{2+} was higher at pH 6.9 compared to that of pH 4.2, which was expected as decreasing the pH led to neutralize the surface charge. It is to be noted that carboxylate ions (–COO^-) are favorable for adsorbing Pb^{2+} species than the charge less –COOH. The JSAC (prior to functionalization) was used for removing Pb^{2+} with various concentrations (0.1–10 ppm) to explain the effect of carboxylic acid functionalization. The removal efficiencies of Pb^{2+} were very low (25–40%) although the morphologies of the JSAC and JSAC-COO^- were similar. However, carboxylic functionalization of JSAC improved the Pb^{2+} removal efficiency significantly. Because of the presence of macro- and mesopores in JSAC-COO^-, the structure made it highly porous in comparison to JSAC, which offered increased binding sites (–COO^-) for Pb^{2+} and increased the removal efficiency of Pb^{2+}.

The particle size, adsorption capacity, and BET surface area of different AC employed in removing Pb^{2+} are presented in Table 3. The particle size of JSAC-COO^- varied from few micrometers to 60 μm. The higher surface area of JSAC-COO^- (615.3 m^2/g) (Table 2) following carboxylic functionalization have improved the performance in removing Pb^{2+} from aqueous solution. The adsorption capacity of JSAC-COO^- was up to 25.0 mg/g within 30 min of contact time while the maximum adsorption capacity is likely to be higher. Approximately 1.0 g/L of JSAC-COO^- removed

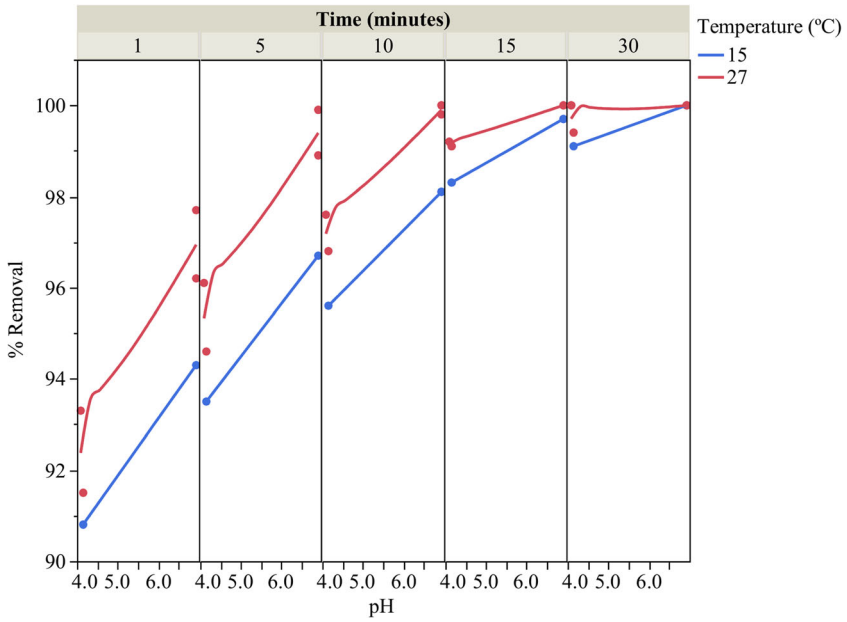

Fig. 9 Effect of pH and temperature on lead removal efficiency

Table 3 Comparison of efficiency and other parameters of JSAC-COO^- with other activated carbons

Adsorbent	Maximal capacity (mg/g)	Particle size	BET surface area (m^2/g)	Reference
GAC with bacteria	26.40	2500 μm	1089	Rivera-Utrilla et al. (2003)
Carbon nanotubes oxidized with concentrated nitric acid	49.95	Length ranges from hundreds of nanometers to micrometers, average diameter is about 30 nm	145	Li et al. (2004)
Coconut shell AC	26.50	75–850 μm	265.96	Sekar et al. (2004)
Sulfur-functionalized coconut shell AC	29.44	8–20 mesh, i.e., 2380–841 μm	900	Goel et al. (2005)
H_2SO_4-treated dates stone AC	19.64	< 125 μm	307.8	Mouni et al. (2010)
H_3PO_4-treated sea-buckthorn stone activated carbon (PASBAC)	51.81	300–425 μm	1071	Mohammadi et al. (2010)
$ZnCl_2$-treated sea-buckthorn stone activated carbon (ZCSBAC)	25.91	300–425 μm	829	Mohammadi et al. (2010)
Apricot stones AC	21.38	125–250 μm	393.2	Mouni et al. (2011)
Powdered pine cone AC	27.53	–	1094.1	Momčilović et al. (2011)
Acid-treated (carboxylated) multiwalled carbon nanotubes (MWCNTs)	166	3 μm length, 3 nm inner diameter, 19 nm outer diameter	194.36	Farghali et al. (2017)
JSAC-COO^-	> 25	Few μm to 60 μm	615.3	Present study. The findings showed the removal efficiency of up to 25 mg/g within 30 min of contact time. The maximum removal efficiency is likely to be higher at equilibrium.

99.8% of Pb^{2+} from an initial concentration of 25 mg/L in 15 min of contact time. Mouni et al. (2011) reported the particle size, surface area, and maximum adsorption capacity of apricot stone activated carbon (AAC) as 125–250 μm, 393.2 m^2/g, and 21.38 mg/g, respectively. For the dates stone AC treated by H_2SO_4, Mouni et al. (2010) reported the particle size, surface area, and adsorption capacity as < 125 μm, 307.8 m^2/g, and 19.64 mg/g, respectively. The sulfur-functionalized coconut shell AC (SAC) exhibited the maximum adsorption capacity of 29.44 mg/g with particle size of 841–2380 μm (Goel et al. 2005). The particle size, surface area, and maximum adsorption capacity of coconut shell activated carbon (CSC) were reported to be 75–850 μm, 265.96 m^2/g, and 26.50 mg/g, respectively (Sekar et al. 2004). In 105 min of contact time, Pb^{2+} removal were reported to be 92.5% and 91% for the initial concentrations of 10 and 20 mg/L of Pb^{2+}, respectively (Sekar et al. 2004). For 30, 40, and 50 mg/L of Pb^{2+}, the removal efficiencies were 89.7%, 84.9%, and 76.9%, respectively, with a contact time of 120 min (Sekar et al. 2004). The H_3PO_4-treated sea-buckthorn stone activated carbon (PASBAC) was reported to have the particle size, surface area, and maximum adsorption capacity of 300–425 μm, 1071 m^2/g, and 51.81 mg/g, respectively. The $ZnCl_2$-treated sea-buckthorn stone activated carbon (ZCSBAC) showed similar removal efficiency with almost half of the adsorption capacity (Mohammadi et al. 2010). The maximum removal efficiencies were in the range of 98.3–98.5% for an initial concentration of 50 mg/L and contact time of 40 min. Sekar et al. (2004) reported the increase in removal efficiency by decreasing particle size, due to the fact that the smaller particles had higher specific surface area available for adsorption (Sekar et al. 2004). For an initial concentration of 20 mg/L of Pb^{2+}, the removal efficiency was increased from 42 to 99% when the particle size of CSC was decreased from 850 to 75 μm (Sekar et al. 2004). The maximum adsorption capacity of multi-walled carbon nanotubes (MWCNTs) was 166 mg/g (Farghali et al. 2017). However, the use of carbon nanotubes in water treatment technology is limited due to the high cost of CNT (Upadhyayula et al. 2009). The commercial value of MWCNT was reported to be US$129/g (Sigma-Aldrich 2019). The adsorption capacity of JSAC-COO^- was comparable to many adsorbents (Table 3). However, the contact time for JSAC-COO^- was much lower than the other adsorbents, which is an advantage over the other adsorbents.

The World Health Organization and Health Canada have set the guideline values for lead concentration in drinking water to 10 μg/L (WHO 2011; Health Canada 2015). The

USEPA has set the action level to 15 μg/L (USEPA 2009). Patterson reported the typical concentrations of lead in drinking water and wastewater generated from the battery manufacturing, acid mine drainage, tailing pond, and steel production plants in the range of 0.5–25 mg/L, which are within the limits of current experiments (Patterson 1985). The JSAC-COO^- adsorbent was produced from jute stick, which is an inexpensive agricultural byproduct and abundant in the South and Southeast Asian countries. The preparation of activated carbon from jute stick and functionalization to produce JSAC-COO^- were relatively simple, indicating the feasibility of mass-scale production for domestic and industrial applications. Being an agricultural by-product, cost of raw material (e.g., jute stick) is likely to be negligible and the overall production cost is likely to be low. However, future study is needed to estimate the cost of JSAC-COO^- through the applications for the domestic and industrial wastewater treatment. In addition, JSAC-COO^- can be tested for coremoval of multiple heavy metals from drinking water and wastewater.

Conclusions

Removal of lead from drinking water, and domestic and industrial wastewater has been an issue. The industrial wastewater may contain very high concentrations of lead, which can contaminate the sources of drinking water. In addition, drinking water from the tap in house might contain higher concentrations of lead than the water distribution system. Lead can induce several health effects upon exposure to low dose for a long period. The carboxylated jute stick activated carbon (JSAC-COO^-) has shown the potential for removing more than 90% of aqueous phase Pb^{2+} ions within 1 min of contact time. In 15 min of contact time, up to 99.8% removal of Pb^{2+} ions was achieved. The JSAC-COO^- showed excellent efficiency within the operational ranges of pH and temperature in the water supply systems, which can reduce the treatment cost further. The adsorbent can be applied for wide ranges of initial concentrations, pH, and temperature, which is advantageous. The adsorbent is applicable to both domestic and industrial scales. Future study is needed to estimate the cost for mass-scale production and application in domestic and industrial sectors. Furthermore, toxicity of the JSAC-COO^- should be investigated as the amount of acid needed in the process of carboxylation might impact the toxicity of JSAC-COO^-. Despite these limitations, the proposed adsorbent sheds light on the fast removal of lead from aqueous solution.

Acknowledgments This work is financially supported by the Deanship of Scientific Research (DSR) at King Fahd University of Petroleum & Minerals (KFUPM) through project no. RG 1409-1 & 2.

References

Adenuga AA, Truong L, Tanguay RL, Remcho VT (2013) Preparation of water soluble carbon nanotubes and assessment of their biological activity in embryonic zebrafish. Int J Biomed Nanosci Nanotechnol 3(1–2):38–51

Ahammad AJS, Odhikari N, Shah SS, Hasan MM, Islam T, Pal PR, Qasem MAA, Aziz MA (2019) Porous tal palm carbon nanosheets: preparation, characterization and application for the simultaneous determination of dopamine and uric acid. Nanoscale Adv 1:613–626. https://doi.org/10.1039/C8NA00090E

Anitha K, Namsani S, Singh JK (2015) Removal of heavy metal ions using a functionalized single-walled carbon nanotube: a molecular dynamics study. J Phys Chem A 119(30):8349–8358

Asadullah M, Jahan I, Ahmed MB, Adawiyah P, Malek HN, Rahman MS (2014) Preparation of microporous activated carbon and its modification for arsenic removal from water. J Ind Eng Chem 20:887–896

Atkinson BW, Bux F, Kasan HC (1998) Considerations for application of biosorption technology to remediate metal-contaminated industrial effluents. Water SA 24(2):129–135

Aziz MA, Yang H (2008) Surfactant and polymer-free electrochemical micropatterning of carboxylated multi-walled carbon nanotubes on indium tin oxide electrodes. Chem Commun 2008:826–828

Banerjee TD, Middleton F, Faraone SV (2007) Environmental risk factors for attention-deficit hyperactivity disorder. Acta Paediatr 96(9): 1269–1274. https://doi.org/10.1111/j.1651-2227.2007.00430.x

Bellinger DC (2008) Very low lead exposures and children's neurodevelopment. Curr Opin Pediatr 20(2):172–177. https://doi.org/10.1097/MOP.0b013e3282f4f97b

Bellinger D, Leviton A, Waternaux C, Needleman H, Rabinowitz M (1987) Longitudinal analyses of prenatal and postnatal lead exposure and early cognitive development. N Engl J Med 316(17):1037–1043. https://doi.org/10.1056/NEJM198704233161701

Benjelloun M, Tarrass F, Hachim K, Medkouri G, Benghanem MGG, Ramdani B (2007) Chronic lead poisoning: a "forgotten" cause of renal disease. Saudi J Kidney Dis Transpl 18(1):83–86

Burmistrov IN, Muratov DS, Ilinykh IA, Kolesnikov EA, Godymchuk AY, Kuznetsov DV (2016) The effects of liquid-phase oxidation of multiwall carbon nanotubes on their surface characteristics. IOP Conf Ser Mater Sci Eng 112:012004. https://doi.org/10.1088/1757-899X/112/1/012004

Cañete-Rosales P, Ortega V, Álvarez-Lueje A, Bollo S, González M, Ansón A, Martínez MT (2012) Influence of size and oxidative treatments of multi-walled carbon nanotubes on their electrocatalytic properties. Electrochim Acta 62:163–171

Carmo M, Linardi M, Poco JGR (2009) Characterization of nitric acid functionalized carbon black and its evaluation as electrocatalyst support for direct methanol fuel cell applications. Appl Catal A Gen 355(1–2):132–138

Chaney RL, Hundemann PT (1979) Use of peat moss columns to remove cadmium from wastewater. J Water Pollut Control Fed 51(1):17–21

Chowdhury S, Mazumder MAJ, Al-Attas O, Husain T (2016) Heavy metals in drinking water: occurrences, implications, and future needs in developing countries. Sci Total Environ 569–570:476–488. https://doi.org/10.1016/j.scitotenv.2016.06.166

Davis WF (1990) A case study of lead in drinking water: protocol, methods, and investigative techniques. Am Ind Hyg Accoc J 51: 620–624

El-Shafey EI, Ali SNF, Al-Busafi S, Al-Lawati HAJ (2016) Preparation and characterization of surface functionalized activated carbons from date palm leaflets and application for methylene blue removal. J Environ Chem Eng 4(3):2713–2724

FAO (Food and Agricultural Organization) (2019) Future fibres. Available at: http://www.fao.org/economic/futurefibres/fibres/jute/en/. Accessed 9 Jan 2018

Farghali AA, Tawab HAA, Moaty SAA, Khaled R (2017) Functionalization of acidified multi-walled carbon nanotubes for removal of heavy metals in aqueous solutions. J Nanostruct Chem 7:101–111

Fraser S, Muckle G, Després C (2006) The relationship between lead exposure, motor function and behaviour in Inuit preschool children. Neurotoxicol Teratol 28:18–27. https://doi.org/10.1016/j.ntt.2005.10.008

Goel J, Kadirvelu K, Rajagopal C, Garg VK (2005) Removal of lead(II) by adsorption using treated granular activated carbon: batch and column studies. J Hazard Mater 125:211–220. https://doi.org/10.1016/j.jhazmat.2005.05.032

Gosset T, Trancart JL, Thevenot DR (1986) Batch metal removal by peat - kinetics and thermodynamics. Water Res 20:21–26

Guo YP, Rockstraw DA (2007) Physicochemical properties of carbons prepared from pecan shell by phosphoric acid activation. Bioresour Technol 98:1513–1521

Gupta VK, Mohan D, Sharma S (1998) Removal of lead from wastewater using bagasse fly ash - a sugar industry waste material. Sep Sci Technol 33:1331–1343

Health Canada (2015) Guidelines for Canadian drinking water quality. Water and Air Quality Bureau, Healthy Environments and Consumer Safety Branch, Health Canada, Ottawa, Ontario. Available online at: https://www.canada.ca/en/healthcanada/services/environmental-workplace-health/waterquality/drinking-water/canadian-drinking-water-guidelines.html. Accessed 12 June 2017

IARC (International Agency for Research on Cancer) (2018) List of classifications: Volume 1–123. Available at: https://monographs.iarc.fr/wp-content/uploads/2018/09/List_of_Classifications.pdf. Accessed 17 Nov 2018

Islam MR, Nurunnabi M, Islam MN (2003) The fuel properties of pyrolytic oils derived from carbonaceous solid wastes in Bangladesh. J Teknol 38(A):75–89 © Universiti Teknologi Malaysia

Johns MM, Toles CA, Marshall WE (2003) Activated carbons from low-density agricultural waste. United States Patent Application 834051

José SC, José S (2006) Lead: chemistry, analytical aspects, environmental impact and health effects, 1st ed. Elsevier

Kalavathy MH, Karthikeyan T, Rajgopal S, Miranda LR (2005) Kinetic and isotherm studies of cu(II) adsorption onto H_3PO_4-activated rubber wood sawdust. J Colloid Interface Sci 292(2):354–362

Khalid N, Ahmad S, Kiani SN, Ahmed J (1998) Removal of lead from aqueoussolution using rice husk. Sep Sci Technol 33(15):2349–2362

Kobya M, Demirbas E, Senturk E, Ince M (2005) Adsorption of heavy metal ions from aqueous solutions by activated carbon prepared from apricot stone. Bioresour Technol 96(13):1518–1521

Lee M, Lee SH, Park JM, Yang J (1998) Removal of lead in a fixed bed column packed with activated carbon and crab shell. Sep Sci Technol 33(7):1043–1056

Lekgoathi MSD, Heveling J, Augustyn WG, Husselman SJ, Masha PG, Rossouw S (2008) Effect of carboxylate functional groups on the surface area of SWCNTs. Int J Nanotechnol Appl 2(2):141–148

Li Y, Di Z, Luan Z, Ding J, Zuo H, Wu X, Xu C, Wu D (2004) Removal of heavy metals from aqueous solution by carbon nanotubes: adsorption equilibrium and kinetics. J Environ Sci 16(2):208–211

Li J-C, Ma Z, Chi Y, Guo SP (2017) The electrochemical properties of one-pot prepared Fe_2SSe/porous carbon composite as anode material for lithium-ion batteries. J Mater Sci 52(3):1573–1580

Martins IJ, Hone E, Foster JK, Sunram-Lea SI, Gnjec A, Fuller SJ, Nolan D, Gandy SE, Martins RN (2006) Apolipoprotein E, cholesterol metabolism, diabetes, and the convergence of risk factors for Alzheimer's disease and cardiovascular disease. Mol Psychiatry 11:721–736. https://doi.org/10.1038/sj.mp.4001854

Merzouk B, Gourich B, Sekki A, Madani K, Chibane M (2008) Removal turbidity and separation of heavy metals using electrocoagulation–electroflotation technique: a case study. J Hazard Mater 164(1):215–222. https://doi.org/10.1016/j.jhazmat.2008.07.144

Meunier N, Drogui P, Montañe C, Hausler R, Mercier G, Blais JF (2006) Comparison between electrocoagulation and chemical precipitation for metals removal from acidic soil leachate. J Hazard Mater 137(1):581–590

Mitra, B.C., 1999. Data book on jute. National Institute of Research on Jute and Allied Fibre Technology (NIRJAFT), Kolata

Mohamed M, Mohand SO, Marc L, Louis CM (2008) Removal of lead from aqueous solutions with a treated spent bleaching earth. Hazard Mater 159:358–364

Mohammadi SZ, Karimi MA, Afzali D, Mansouri F (2010) Removal of Pb(II) from aqueous solutions using activated carbon from sea-buckthorn stones by chemical activation. Desalination 262(1–3):86–93. https://doi.org/10.1016/j.desal.2010.05.048

Momčilović M, Purenović M, Bojić A, Zarubica A, Randelovid M (2011) Removal of lead(II) ions from aqueous solutions by adsorption onto pine cone activated carbon. Desalination 276:53–59. https://doi.org/10.1016/j.desal.2011.03.013

Mouni L, Merabet D, Bouzaza A, Belkhiri L (2010) Removal of Pb^{2+} and Zn^{2+} from the aqueous solutions by activated carbon prepared from dates stone. Desalin Water Treat 16:66–73. https://doi.org/10.5004/dwt.2010.1106

Mouni L, Merabet D, Bouzaza A, Belkhiri L (2011) Adsorption of Pb(II) from aqueous solutions using activated carbon developed from apricot stone. Desalination 276:148–153. https://doi.org/10.1016/j.desal.2011.03.038

Navas-Acien A, Guallar E, Silbergeld EK, Rothenberg SJ (2007) Lead exposure and cardiovascular disease - a systematic review. Environ Health Perspect 115(3):472–482

Netzer A, Hughes DE (1984) Adsorption of copper, lead and cobalt by activated carbon. Water Res 18(8):927–933

Patterson JW (1985) Industrial wastewater treatment technology, 2nd edn. Butterworth Publishers, Stoneharn

Patrick L (2006) Lead toxicity part II: The role of free radical damage and the use of antioxidants in the pathology and treatment of lead toxicity. Altern Med 11:114–127

Quan J, Yong-jian W, Ying-liang L (2012) Synthesis and characterization of graphitic carbon with hollow structures. New Carbon Mater 27:123–128

Rivera-Utrilla J, Bautista-Toledo I, Ferro-Garcıa MA, Moreno-Castilla C (2003) Bioadsorption of Pb (II), Cd (II), and Cr (VI) on activated carbon from aqueous solutions. Carbon 41(2):323–330

Sekar M, Sakthi V, Rengaraj S (2004) Kinetics and equilibrium adsorption study of lead(II) onto activated carbon prepared from coconut shell. J Colloid Interface Sci 279:307–313. https://doi.org/10.1016/j.jcis.2004.06.042

Sigma Aldrich (2019) Sigma Aldrich. Available at: https://www.sigmaaldrich.com/catalog/product/aldrich/755125?lang=en®ion=US. Accessed 16 Oct 2018

Sun YN, Sui ZY, Li X, Xiao PW, Wei ZX, Han B-H (2018) Nitrogen-doped porous carbons derived from polypyrrole-based aerogels for gas uptake and supercapacitors. ACS Appl Nano Mater 1:609–616

Tan IAW, Ahmad AL, Hameed BH (2008) Adsorption of basic dye on high surface-area activated carbon prepared from coconut husk: equilibrium, kinetic and thermodynamic studies. J Hazard Mater 154:337–346

Tejada C, Herrera A, Ruiz E (2016) Kinetic and isotherms of biosorption of Hg(II) using citric acid treated residual materials. Ing Compet 18:117–127

Thommes M, Kaneko K, Alexander VN, James PO, Rodriguez-Reinoso F, Rouquerol J, Kenneth SWS (2015) Physisorption of gases, with special reference to the evaluation of surface area and pore size distribution (IUPAC Technical Report). Pure Appl Chem 87:1051–1069

Upadhyayula VKK, Deng S, Mitchell MC, Smith GB (2009) Application of carbon nanotube technology for removal of contaminants in drinking water: a review. Sci Total Environ 408:1–13

USEPA (United States Environmental Protection Agency) (1998) Method 6020A: inductively coupled plasma - mass spectrometry

USEPA (United States Environmental Protection Agency) (2004) Lead and compounds (inorganic) (CASRN 7439-92-1) 1–15

USEPA (United States Environmental Protection Agency) (2009) National primary drinking water regulations 1

USEPA (United States Environmental Protection Agency) (2012) Basic information about lead in drinking water [WWW document]. Environ Prot Agency. URL http://water.epa.gov/drink/contaminants/basicinformation/lead.cfm. Accessed 20 Oct 2018

Wang Q, Zhang C, Shen G, Liu H, Fu H, Cui D (2014) Fluorescent carbon dots as an efficient siRNA nanocarrier for its interference therapy in gastric cancer cells. J Nanobiotechnol 12(58):58. https://doi.org/10.1186/s12951-014-0058-0

Wani AL, Ara A, Usmani JA (2015) Lead toxicity: a review. Interdiscip Toxicol 8:55–64. https://doi.org/10.1515/intox-2015-0009

Weng CH, Huang CP (1994) Treatment of metal industrial wastewater by fly ash and cement fixation. J Environ Eng ASCE 120:1470–1487

WHO (World Health Organization) (2003) Lead in drinking-water. Guidel Drink Qual 9:1–7. https://doi.org/10.1155/2013/959637

WHO (World Health Organization) (2011) Guidelines for drinking-water quality – 4th ed., Geneva, Switzerland. Available online at: https://www.who.int/water_sanitation_health/publications/2011/dwq_guidelines/en/. Accessed 15 June 2017

Wilson W, Yang H, Seo CW, Marshall WE (2006) Select metal adsorption by activated carbon made from peanut shells. Bioresour Technol 97:2266–2270

Yu DY, Xu ZR, Yang XG (2006) In vitro, in vivo studies of Cu(II)-exchanged montmorillonite for the removal of lead (Pb). Anim Feed Sci Technol 127:327–335